

ON THE DISINTEGRATION OF ICE SHELVES: THE ROLE OF FRACTURE

By T. HUGHES

(Department of Geological Sciences and Institute for Quaternary Studies, University of Maine at Orono, Orono, Maine 04469, U.S.A.)

ABSTRACT. Crevasses can be ignored in studying the dynamics of most glaciers because they are only about 20 m deep, a small fraction of ice thickness. In ice shelves, however, surface crevasses 20 m deep often reach sea-level and bottom crevasses can move upward to sea-level (Clough, 1974; Weertman, 1980). The ice shelf is fractured completely through if surface and basal crevasses meet (Barrett, 1975; Hughes, 1979). This is especially likely if surface melt water fills surface crevasses (Weertman, 1973; Pfeffer, 1982; Fastook and Schmidt, 1982). Fracture may therefore play an important role in the disintegration of ice shelves. Two fracture criteria which can be evaluated experimentally and applied to ice shelves, are presented. Fracture is then examined for the general strain field of an ice shelf and for local strain fields caused by shear rupture alongside ice streams entering the ice shelf, fatigue rupture along ice shelf grounding lines, and buckling up-stream from ice rises. The effect of these fracture patterns on the stability of Antarctic ice shelves and the West Antarctic ice sheet is then discussed.

RÉSUMÉ. *Sur la désintégration des plateformes glaciaires: Le rôle de la fracturation.* Dans l'étude de la dynamique de la plupart des glaciers on peut négliger l'action des crevasses parce que leur profondeur, seulement de l'ordre de 20 m, n'est qu'une faible fraction de l'épaisseur totale de glace. Dans la plateforme glaciaire, au contraire, les crevasses de surface peuvent atteindre le niveau de la mer et les crevasses de fond remonter jusqu'à ce niveau (Clough, 1974; Weertman, 1980). La plateforme est fracturée de part en part si les crevasses de fond et de surface se rencontrent (Barrett, 1975; Hughes, 1979). Ceci est spécialement fréquent si l'eau de fusion remplit les crevasses de surface (Weertman, 1973; Pfeffer, 1982; Fastook et Schmidt, 1982). La fracturation peut donc jouer un rôle important dans la désintégration de la plateforme. On présente deux indicateurs de fracturation qui peuvent être estimés expérimentalement et appliqués aux plateformes glaciaires. La fracturation est alors examinée en fonction du champ général des contraintes dans une masse de glace, des champs de contraintes locaux causés par les ruptures au cisaillement le long des fluxes de glace entrant la plateforme, les ruptures dues à la fatigue le long de la ligne de décollement du sol, la poussée vers l'amont due aux domes insulaires de glace. L'effet de ces types de fracturation sur la stabilité des plateformes glaciaires de l'Antarctique et de la calotte glaciaire Ouest Antarctique est ensuite discuté.

ZUSAMMENFASSUNG. *Über die Auflösung von Schelfeisen: Die Rolle der Bruchbildung.* Dynamische Studien können bei den meisten Gletschern deren Spalten ausser Betracht lassen, da deren Tiefe nur etwa 20 m, also einen kleinen Bruchteil der Eisdicke, beträgt. In Schelfeisen jedoch reichen 20 m tiefe Oberflächenspalten oft bis auf das Meeresniveau, während Spalten am Untergrund sich bis zum Meeresspiegel nach oben öffnen können (Clough, 1974; Weertman 1980). Das Schelfeis bricht völlig durch, wenn sich Spalten von oben und unten treffen (Barrett, 1975; Hughes, 1979). Dies ist besonders wahrscheinlich, wenn Schmelzwasser Oberflächenspalten füllt (Weertman, 1973; Pfeffer, 1982; Fastook und Schmidt, 1982). Spaltenbildung dürfte daher eine wesentliche Rolle bei der Auflösung von Schelfeisen spielen. Es werden zwei Bruchkriterien, die experimentell ausgewertet und auf Schelfeise angewandt werden können, dargestellt. Die Bruchbildung wird dann für das allgemeine Spannungsfeld eines Schelfeises und für lokale Spannungsfelder, verursacht durch Scherbrüche längs Eisströmen, die dem Schelfeis zufließen, durch Ermüdungsbrüche längs Abhublinien des Schelfeises und durch Aufwärtsströmen an Eisaufwölbungen untersucht. Die Wirkung dieser Bruchmuster auf die Stabilität antarktischer Schelfeise und auf den westantarktischen Eisschild wird diskutiert.

INTRODUCTION

Fracture is a process that has received little attention among glaciologists, but it may be a critical process in ice-shelf dynamics. Since both surface and basal crevasses exist in ice shelves,

and they can join to fracture the whole ice thickness (Barrett, 1975; Hughes, 1979), a fracture criterion that can be applied to ice shelves should be developed. Figure 1 shows the distribution of Antarctic ice shelves. The CLIMAP ice-sheet disintegration model predicts that the marine West Antarctic ice sheet would collapse were it not buttressed by ice shelves (Stuiver and others, 1981). Disintegration of these buttressing ice shelves would probably be controlled by fracture.

Figure 2 shows the kinds of fracture patterns that exist in Antarctic ice shelves. Shear rupture crevasses are shown alongside the floating tongue of Byrd Glacier (1), shear/fatigue rupture crevasses are shown around Crary Ice Rise (2) and in Fashion Lane along the Shirase Coast (3), radial crevasses are shown for bending converging flow around Minna Bluff (4) and for radially diverging flow in the freely-floating tongue of Stancomb-Wills Glacier (6), and transverse crevasses are shown in the Grand Chasms of Filchner Ice Shelf (5). Crevasses

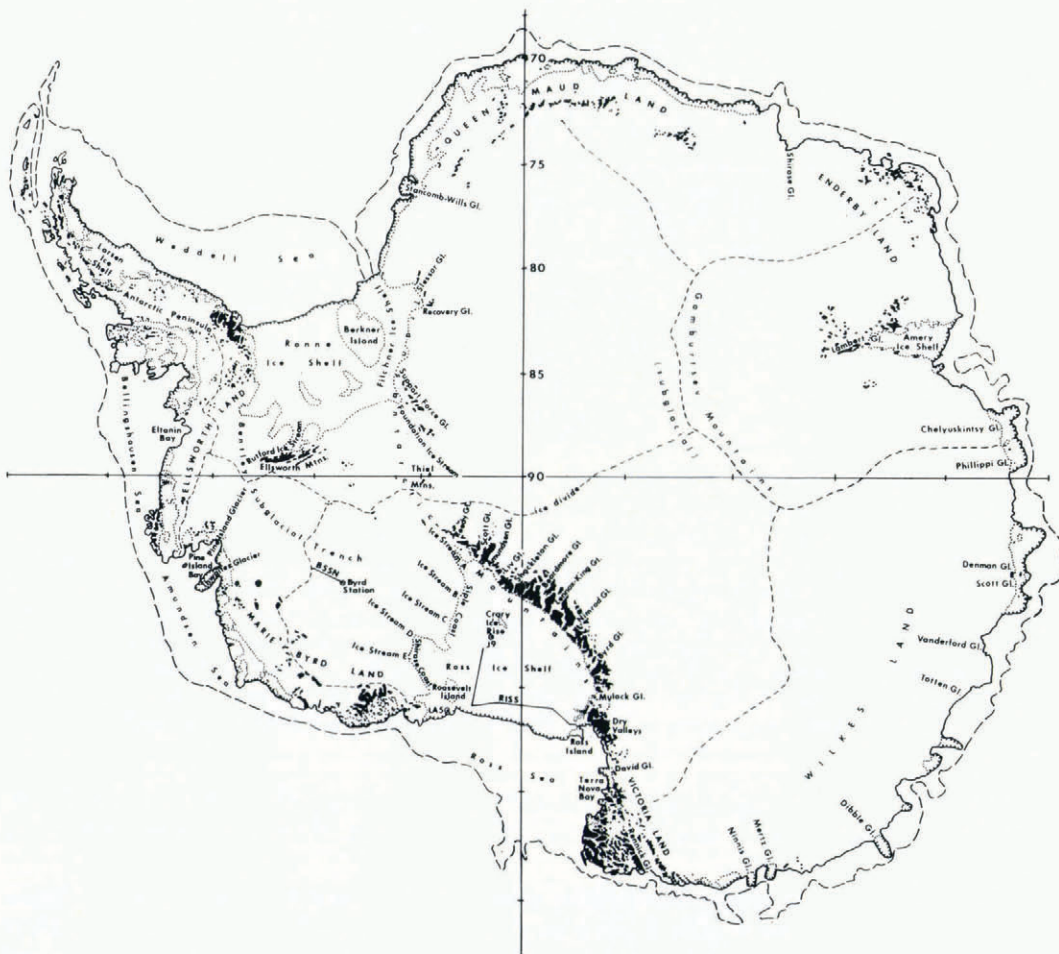


Fig. 1. Antarctic identification map. Shown are the edge of the continental shelf (broken line), tidewater calving margins (solid line), ice-shelf calving margins (hatched lines), ice-shelf grounding lines (dotted lines), ice divides (dashed lines), and regions of mountain glaciation (black areas).

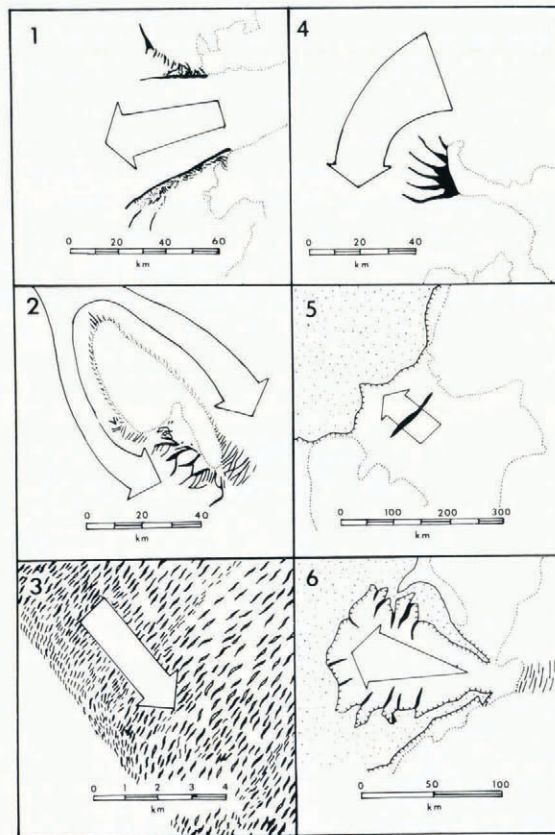


Fig. 2. Characteristic crevasse patterns in Antarctic ice shelves. Crevasses associated with weak links include shear rupture alongside the floating tongues of ice streams (1, lateral rifts of Byrd Glacier tongue, long. 161° E., lat. 80.2° S., Hughes, 1977), fatigue rupture around ice rises (2, "horst and graben" rifts in the lee of Cray Ice Rise, long. 171° W., lat. 83° S., Barrett, 1975), shear-fatigue rupture along lateral grounding lines (3, "Fashion Lane" along the Shirase Coast, long. 151° W., lat. 79.5° S., Thiel and Ostenso, 1975). Crevasses associated with the general strain field include shear crevasses from bending converging flow (4, radial crevasses around Minna Bluff, long. 167° E., lat. 78.5° S., see Hughes, 1977, fig. 26f), transverse crevasses from straight parallel flow (5, The Grand Chasms on the Filchner Ice Shelf, long. 40° W., lat. 78.7° S., American Geographical Society, 1970), and longitudinal crevasses from radially diverging flow (6, crevasses normal to the calving front of Stancomb-Wills Glacier Tongue (long. 22° W., lat. 75.0° S., American Geographical Society, 1970).

disintegrate the ice shelf along its calving front and weaken its links to the ice streams that feed it, to the ice rises that anchor it to the sea floor, and to the sides of the embayment where it is confined.

The fracture criterion used in this paper is based on the concept of a critical fracture strain. Strain energy accumulated at grain boundaries in polycrystalline ice is released when a critical strain triggers viscoplastic instability. Strain energy is relieved rapidly by fracture and slowly by recrystallization. Ice moving from the grounding line to the calving front of an ice shelf passes through a strain field that is constantly changing as a result of both general flow and deformation at weak links. Strain energy in the moving ice is minimized if the ice fabric changes continuously

in order to be always compatible with the changing strain field, thereby obeying Neumann's Principle (Nye, 1960, p. 20–24, p. 104). An ice fabric that is stable for a given strain field becomes metastable as the strain field changes and is unstable when strain energy is maximized at a critical strain. Further strain causes fracture or recrystallization. Recrystallization reduces strain energy by creating a new ice fabric that is stable in the new strain field. Strain hardening and primary creep occur before recrystallization. Strain softening and tertiary creep occur during recrystallization. The critical strain is the strain of viscoplastic instability. If this strain requires a stress that exceeds the fracture stress, the ice will crack instead of recrystallizing. Crevasses open on ice shelves where strain energy is reduced by fracture instead of by recrystallization. Tertiary creep reflects both recrystallization and crack propagation.

Figure 3 shows schematically how strain ε varies with strain energy E , stress σ , and time t during a recrystallization episode as ice moves through the changing strain field of an ice shelf. The flow curve shows the variation of σ with ε , where $d\sigma/d\varepsilon$ is positive during strain hardening and negative during strain softening. Strains for which $d\sigma/d\varepsilon = 0$ exist at an upper yield stress where recrystallization begins and a lower yield stress where recrystallization ends. Fracture and crevassing, if present, begin at the upper yield stress. The creep curve shows the variation of ε with t , where strain-rate $\dot{\varepsilon}$ decreases during primary creep and increases during tertiary creep. Secondary creep occurs when $\dot{\varepsilon}$ is constant during stable and unstable steady-state flow. Unstable flow occurs when strain hardening is exactly cancelled by strain softening at the beginning of recrystallization, and results in slow secondary creep. Stable flow occurs after recrystallization is complete, and results in fast secondary creep. Crevasses that open during slow secondary creep propagate through the ice shelf during tertiary creep.

Three common constitutive equations are used to relate stress σ , strain ε , strain-rate $\dot{\varepsilon}$, and time t to each other in Figure 3. For the flow curve:

$$\varepsilon = (\sigma/\sigma_s)^s \quad (1)$$

where $\dot{\varepsilon}$ is kept constant (Dieter, 1961, p. 247). For the creep curve:

$$\varepsilon = (\dot{\varepsilon}_c t)^c \quad (2)$$

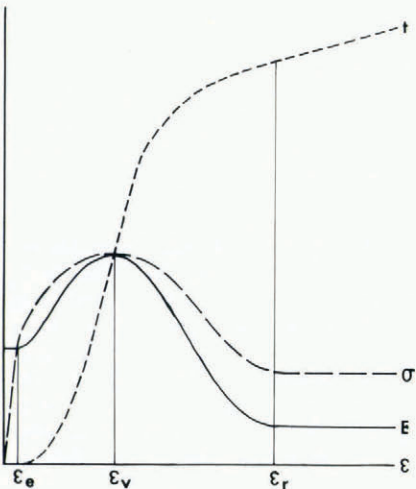


Fig. 3. Conditions for recrystallization or fracture in polycrystalline ice. The dependence of strain ε with strain energy E , stress σ , and time t has critical values at the elastic limit strain ε_e when strain hardening and transient creep begin, at the strain of viscoplastic instability ε_v when strain softening and recrystallization begin, and at strain ε_r when strain softening and recrystallization end. Metastable equilibrium exists until ε_e , unstable equilibrium exists at ε_v , and stable equilibrium exists beyond ε_r . Fracture occurs if recrystallization is unable to relieve the strain energy, with brittle fracture occurring instantaneously at ε_v and ductile fracture occurring progressively from ε_v onward.

where σ is kept constant (Dieter, 1961, p. 348). For the steady-state or secondary creep:

$$\dot{\epsilon} = (\sigma/A)^n \tag{3}$$

where $d\dot{\epsilon}/dt = 0$ (Dieter, 1961, p. 350). Temperature T is kept constant in Equations (1) through (3). σ_s is a strength coefficient, s is a strength exponent, $\dot{\epsilon}_c$ is a strain-rate coefficient, c is a creep exponent, A is a hardness coefficient, and n is a viscoplastic exponent. For elastic strain, σ_s is the elastic modulus and $s = 1$. For viscoplastic strain, σ_s is a viscoplastic modulus, $\sigma = \sigma_v$ is an upper yield stress when viscoplastic instability triggers recrystallization, $\sigma = \sigma_r$ is a lower yield stress when recrystallization is complete, $s \rightarrow 0$ at these yield stresses, $s > 1$ during strain hardening, $s < 0$ during strain softening, $0 < c < 1$ during primary creep, $c = 1$ during both slow and fast secondary creep, and $c > 1$ during tertiary creep.

Figure 4 shows the viscoplastic spectrum for secondary steady-state creep, and illustrates the basis for two fracture criteria. In the viscoplastic creep spectrum, $n = 1$ and $A = \eta_0$ is the fluid viscosity for viscous flow and $n = \infty$ and $A = \sigma_0$ is the yield stress for plastic flow. The effective viscosity for viscoplastic flow is obtained by differentiating Equation (3):

$$\eta_v = \frac{d\sigma}{d\dot{\epsilon}} = \frac{A^n}{n\sigma^{n-1}} = \frac{\sigma}{n\dot{\epsilon}} = \frac{\eta_0}{n} \tag{4}$$

Equation (4) is plotted in Figure 5.

FRACTURE CRITERIA FOR ICE

Consider principal stresses σ_k where $k = 1, 2, 3$ in tensor notation. Let σ_1 be the maximum principal stress and σ_2 be the minimum principal stress on the surface of an ice shelf. Fracture occurs when the maximum shear stress $\tau_m = \frac{1}{2}(\sigma_1 - \sigma_2)$ reaches the viscoplastic yield stress σ_v . In order to specify σ_v it is useful to rewrite Equation (3) in the form with $\sigma = \tau_m$:

$$\epsilon_m = \epsilon_0 (\tau_m / \sigma_0)^n \tag{5}$$

where σ_0 is the plastic yield stress where viscoplastic instability, followed by recrystallization or

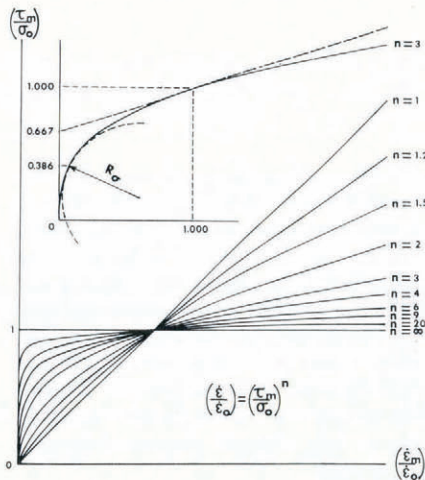


Fig. 4. The viscoplastic spectrum for steady-state creep and two criteria for viscoplastic yielding. A sharp knee develops in stress-strain rate curves when the viscoplastic exponent n increases, where $\dot{\epsilon}_m$ is the strain rate at the maximum shear stress τ_m , $\dot{\epsilon}_0$ is the strain rate at the plastic yield stress σ_0 and $\dot{\epsilon}_m / \dot{\epsilon}_0 = (\tau_m / \sigma_0)^n$. Viscoplastic yielding occurs at the knee in the maximum stress-curvature yield criterion and at the stress intercept of the tangent line at $\dot{\epsilon}_0$ in the critical strain rate yield criterion. For $n = 3$, $\sigma_v = 0.386\sigma_0$ at the knee and $\sigma_v = 0.667\sigma_0$ at the stress intercept.

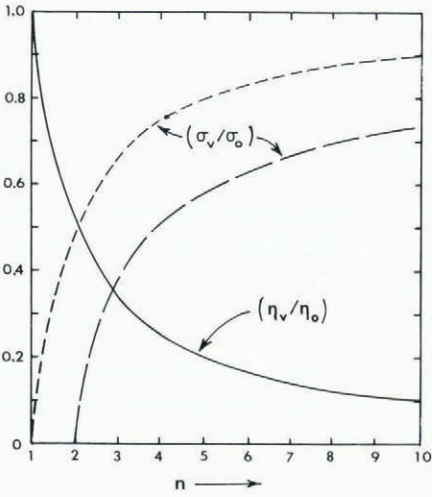


Fig. 5. Variations of yield stress and viscosity across the viscoplastic spectrum of steady-state creep. Ratios of viscoplastic yield stress σ_v and plastic yield stress σ_0 increase with the viscoplastic exponent n according to Equation (8) for the maximum stress-curvature yield criterion (broken curve) and according to Equation (10) for the critical strain-rate yield criterion (dashed curve). The ratio of effective viscosity η_v and fluid viscosity η_0 decreases with increasing n (solid curve).

fracture, occurs at a critical strain-rate

$$\dot{\epsilon}_0 = \frac{(\tau_m/A)^n}{(\tau_m/\sigma_0)^n} = \left(\frac{\sigma_0}{A}\right)^n \tag{6}$$

If recrystallization occurs, strain softening causes τ_m to drop and fracture is prevented. With fracture, $\tau_m = \sigma_v$ is maintained at the tip of an opening crevasse only if the tip moves into the ice.

Figure 4 illustrates two criteria for specifying σ_v . In the maximum stress-curvature criterion, σ_v is the stress at which τ_m changes most rapidly with respect to $\dot{\epsilon}_m$. The radius of stress curvature obtained from Equation (5) is

$$R_\sigma = \frac{\left[1 + \left(\frac{d(\dot{\epsilon}_m/\dot{\epsilon}_0)}{d(\tau_m/\sigma_0)}\right)^2\right]^{3/2}}{\frac{d^2(\dot{\epsilon}_m/\dot{\epsilon}_0)}{d(\tau_m/\sigma_0)^2}} = \frac{[1 + n^2(\tau_m/\sigma_0)^{2n-2}]^{3/2}}{n(n-1)(\tau_m/\sigma_0)^{n-2}} \tag{7}$$

Setting $dR_\sigma/d(\tau_m/\sigma_0) = 0$ at the maximum stress curvature where $\tau_m = \sigma_v$ gives

$$\frac{\sigma_v}{\sigma_0} = \left[\frac{n-2}{2(n-1)n^2}\right]^{1/(2n-2)} \tag{8}$$

In the critical strain-rate criterion, σ_v is the value of τ_m at $\dot{\epsilon}_m = 0$ that is obtained at the stress intercept of straight lines that are tangent to curves of (τ_m/σ_0) versus $(\dot{\epsilon}_m/\dot{\epsilon}_0)$ at critical strain-rate $\dot{\epsilon}_m = \dot{\epsilon}_0$. The equation of these straight lines is

$$\frac{\tau_m}{\sigma_0} = \left(\frac{d(\tau_m/\sigma_0)}{d(\dot{\epsilon}_m/\dot{\epsilon}_0)}\right) \frac{\dot{\epsilon}_m}{\dot{\epsilon}_0} + \frac{\sigma_v}{\sigma_0} = \left(\frac{d\tau_m}{d\dot{\epsilon}_m}\right) \frac{\dot{\epsilon}_m}{\dot{\epsilon}_0} + \frac{\sigma_v}{\sigma_0} \tag{9}$$

Setting $\tau_m = \sigma_0$ at $\dot{\epsilon}_m = \dot{\epsilon}_0$ and differentiating Equation (5) to obtain $d\tau_m/d\dot{\epsilon}_m = \sigma_0/n\dot{\epsilon}_0$ gives

$$\frac{\sigma_v}{\sigma_0} = \frac{n-1}{n}. \quad (10)$$

Figure 5 compares Equations (8) and (10) over the same range of n .

The value of σ_0 is related to the value of A , which depends on the density, fabric, texture, and purity of glacial ice. For polycrystalline ice having maximum density ρ_1 and high purity, Baker (1981) has obtained the following relationship between the effective stress τ and the effective strain rate $\dot{\epsilon}$ during steady-state creep:

$$\dot{\epsilon} = Bd^{3.145}f^{0.997}\tau^3 \exp(-Q/kT) \quad (11)$$

where B is a constant, d is crystal size, f is fabric intensity, Q is thermal activation energy, T is absolute temperature, and k is Boltzmann's constant. Density ρ increases substantially with depth through an ice shelf, and hardness increases with density. If $A \propto (\rho/\rho_1)^\kappa$ and $\kappa \simeq 1$, Equation (11) gives

$$A \simeq \left(\frac{\rho}{\rho_1}\right)^\kappa \frac{\exp(Q/3kT)}{(Bd^{3.145}f^{0.997})^{1/3}} \simeq \left(\frac{\rho}{\rho_1}\right) \frac{\exp(Q/3kT)}{B^{1/3}df^{1/3}}. \quad (12)$$

Variations of ρ , d , f , and T with depth in Antarctic ice shelves can be obtained from the data published by Gow (1963).

Laboratory fracture tests can be conducted to determine whether Equation (8) or Equation (10) provides the best fracture criterion for ice. Figure 4 shows that when $\tau_m = \sigma_v$ fracture occurs at $\dot{\epsilon}_m = \dot{\epsilon}_0$ for any value of n when Equation (10) is employed. The value of σ_0 is therefore obtained from Equation (6) for $\dot{\epsilon}_0 = \frac{1}{2}(\dot{\epsilon}_1 - \dot{\epsilon}_2)$ measured at the moment of fracture and A computed from Equation (12) for given values of d , f , and T , where $\rho = \rho_1$ for bubble-free ice. The state of stress also allows $\sigma_v = \frac{1}{2}(\sigma_1 - \sigma_2)$ to be determined at the moment of the fracture. Since $n=3$ for ice, Equation (10) applies if $(\sigma_v/\sigma_0)=0.667$, as determined by fracture experiments. If this test fails, Equation (8) must apply.

FRACTURE FOR SHELF FLOW

Flow in an ice shelf is determined by the geometry of its confining embayment and by the number and location of the ice streams that feed it and the ice rises where it is anchored to the sea floor. Fracture in the ice shelf occurs when its flow pattern results in principal surface stresses such that $\sigma_v = \tau_m = \frac{1}{2}(\sigma_1 - \sigma_2)$. In tensor notation, subscripts i, j, k denote rectilinear axes x, y, z in succession so that

$$\sigma_{ij} = \sigma'_{ij} + \delta_{ij}P \quad (13)$$

where σ_{ij} and σ'_{ij} are components of the stress and the stress deviator, δ_{ij} is the Kronecker delta, and $P = \sigma_{kk}/3$ is hydrostatic pressure. The tensor form of Equation (3) is (Glen, 1958)

$$\dot{\epsilon}_{ij} = (\tau^{n-1}/A^n)\sigma'_{ij} \quad (14)$$

where $\tau = (\frac{1}{2} \sum_{ij} \sigma'_{ij}{}^2)^{1/2}$ is the effective stress. Since $P \rightarrow 0$ at the surface of an ice shelf, $\sigma_1 - \sigma_2 = \sigma'_1 - \sigma'_2 = (A^n/\tau^{n-1})(\dot{\epsilon}_1 - \dot{\epsilon}_2)$ from Equations (13) and (14). Consequently, σ_v can be determined if A , τ , and the principal surface strain-rates are known when a crevasse opens.

Since $\dot{\epsilon}_{ij} \propto \sigma'_{ij}$ in Equation (14), the ratio R of surface strain-rates is

$$R = \frac{\dot{\epsilon}_2}{\dot{\epsilon}_1} = \frac{\sigma'_2}{\sigma'_1} = \frac{\sigma_2 - \frac{1}{3}(\sigma_1 + \sigma_2 + \sigma_3)}{\sigma_1 - \frac{1}{3}(\sigma_1 + \sigma_2 + \sigma_3)}. \quad (15)$$

Solving Equation (15) for σ_2 gives

$$\sigma_2 = \left(\frac{2R + 1}{2 + R} \right) \sigma_1 + \left(\frac{1 - R}{2 + R} \right) \sigma_3. \quad (16)$$

Substituting Equation (16) into the expression for τ in terms of principal stresses gives

$$\begin{aligned} \tau &= \left\{ \frac{1}{6} [(\sigma_1 - \sigma_2)^2 + (\sigma_2 - \sigma_3)^2 + (\sigma_3 - \sigma_1)^2] \right\}^{1/2} \\ &= (1 + R + R^2)^{1/2} \frac{\sigma_1 - \sigma_3}{2 + R}. \end{aligned} \quad (17)$$

Substituting Equation (16) into the expression for σ'_1 in terms of principal stresses gives

$$\sigma'_1 = \sigma_1 - \frac{1}{3}(\sigma_1 + \sigma_2 + \sigma_3) = \frac{\sigma_1 - \sigma_3}{2 + R}. \quad (18)$$

Substituting Equations (17) and (18) into Equation (14) gives the flow law for a horizontal ice shelf in terms of R and its principal stresses σ_1 and σ_3 :

$$\dot{\epsilon}_1 = (1 + R + R^2)^{(n-1)/2} \left[\frac{\sigma_1 - \sigma_3}{(2 + R)A} \right]^n. \quad (19)$$

Terms containing R in Equation (19) can be collected to form a constant R' defined as

$$R' = \frac{(1 + R + R^2)^{(n-1)/2}}{(2 + R)^n}. \quad (20)$$

The principal strain-rates for an ice shelf are then:

$$\dot{\epsilon}_1 = R'(\sigma_1 - \sigma_3)^n / A^n \quad (21a)$$

$$\dot{\epsilon}_2 = R\dot{\epsilon}_1 \quad (21b)$$

$$\dot{\epsilon}_3 = -(\dot{\epsilon}_1 + \dot{\epsilon}_2) = -(1 + R)\dot{\epsilon}_1 \quad (21c)$$

where Equation (21c) expresses the first invariant of strain-rate for conservation of volume ($\dot{\epsilon}_{kk} = 0$).

Since hydrostatic pressure increases linearly with depth for an ice shelf having thickness h_1 and density ρ_1 ,

$$\sigma_3 = \sigma_z = -\rho_1 g(h_1 - z) \quad (22)$$

where g is gravity acceleration and $z = 0$ at the base of the ice shelf. Substituting Equation (22) into Equation (21a) and solving for σ_1 , gives

$$\sigma_1 = A(\dot{\epsilon}_1 / R')^{1/n} - \rho_1 g(h_1 - z). \quad (23)$$

The base of the ice shelf is below sea-level at depth h_w in water of density ρ_w . Balancing

hydrostatic pressure in a given ice column by the hydrostatic pressure of water in the column if the ice melted:

$$\int_0^{h_1} \sigma_1 dz = \int_0^{h_w} \rho_w g(h_w - z) dz. \quad (24)$$

Note that the effect of σ_2' is accounted for by measuring $\dot{\epsilon}_2$ to compute R' . Substituting Equation (23) for σ_1 , integrating, and solving for $\dot{\epsilon}_1$ gives:

$$\dot{\epsilon}_1 = \frac{R'(\frac{1}{2}\rho_1 g h_1^2 - \frac{1}{2}\rho_w g h_w^2)^n}{\left[\int_0^{h_1} A dz\right]^n} = \frac{(1 + R + R^2)^{(n-1)/2}}{(2 + R)^n} \left[\frac{\rho_1 g h_1}{2\bar{A}} \left(1 - \frac{\rho_1}{\rho_w}\right) \right]^n \quad (25)$$

where Equation (20) is substituted for R' , buoyancy requires that $h_w = (\rho_1/\rho_w)h_1$, and the average value of A is:

$$\bar{A} = \frac{1}{h_1} \int_0^{h_1} A dz. \quad (26)$$

Equation (12) incorporates vertical density variations into A in Equation (26). Sanderson (1979) presents an alternative procedure.

Principal strain rates $\dot{\epsilon}_k$ are obtained from strain rates $\dot{\epsilon}_{ij}$ using the Mohr circle construction:

$$\dot{\epsilon}_1 = \frac{1}{2}(\dot{\epsilon}_{xx} + \dot{\epsilon}_{yy}) + \left[\frac{1}{4}(\dot{\epsilon}_{xx} - \dot{\epsilon}_{yy})^2 + \dot{\epsilon}_{xy}^2 \right]^{1/2}, \quad (27a)$$

$$\dot{\epsilon}_2 = \frac{1}{2}(\dot{\epsilon}_{xx} + \dot{\epsilon}_{yy}) - \left[\frac{1}{4}(\dot{\epsilon}_{xx} - \dot{\epsilon}_{yy})^2 + \dot{\epsilon}_{xy}^2 \right]^{1/2}, \quad (27b)$$

$$\tan 2\phi = 2\dot{\epsilon}_{xy}/(\dot{\epsilon}_{xx} - \dot{\epsilon}_{yy}) \quad (27c)$$

where ϕ is the angle between coordinates x, y and 1, 2.

Most Antarctic ice shelves occupy embayments, so ice entering such an ice shelf crosses a grounding line perimeter that is substantially longer than the calving perimeter crossed by ice leaving the ice shelf. Consequently, a typical flowband is bent around the z direction and converges in the x direction. Figure 6 shows bending parallel flow in a flowband at distance r from the bending axis and having constant width Δr . Bending through angle θ changes the arc length an amount Δs across the flowband, which has an average arc length along its centerline of $x' - x''$. If ice converges along this distance, the flowband width decreases uniformly from y' to y'' and the flowband velocity increases uniformly from u' to u'' . The strain and strain-rates for simple shear in the flowband are:

$$\gamma_{xy} = -\Delta s/\Delta r = -\theta \Delta r/\Delta r = -\theta, \quad (28a)$$

$$\dot{\gamma}_{xy} = \dot{\epsilon}_{xy} + \dot{\omega}_{xy} = \frac{1}{2} \left(\frac{\partial u}{\partial y} + \frac{\partial v}{\partial x} \right) + \frac{1}{2} \left(\frac{\partial u}{\partial y} - \frac{\partial v}{\partial x} \right) = \frac{du}{dy} \quad (28b)$$

where the pure shear strain-rate is $\dot{\epsilon}_{xy}$, the rigid body rotation rate is $\dot{\omega}_{xy}$, the velocity along x is u , the velocity along y is v , and $dv/dx = 0$. Consequently, $\dot{\epsilon}_{xy} = \dot{\omega}_{xy} = \frac{1}{2}\dot{\gamma}_{xy} = -\frac{1}{2}\theta$. For flow that bends around z and converges along x , the average horizontal strain-rate components are those

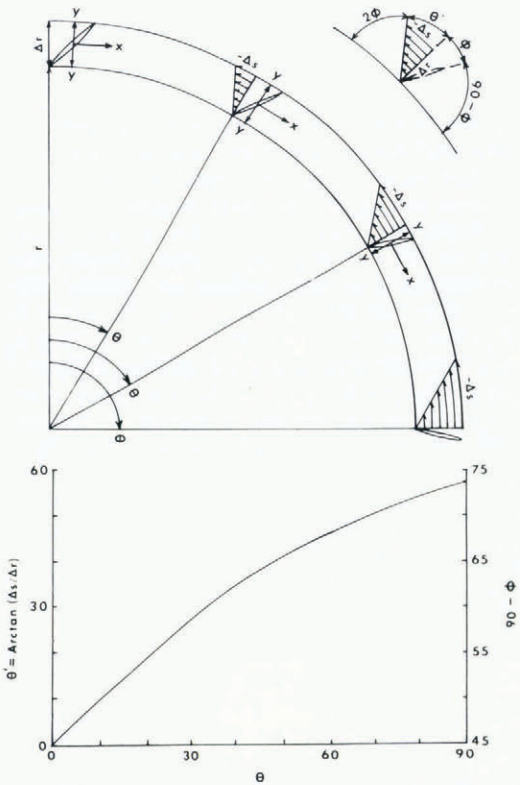


Fig. 6. Bending parallel flow on an ice shelf. In a flowband at distance r from the bending axis and having width Δr , simple shear deformation Δs increases with the angle of bending θ about the bending axis and the angle of shear θ' in the flowband, where $\theta = \Delta s / \Delta r = \tan \theta'$. A crevasse (lens-shaped opening) that initially opens at angle $\phi = 45^\circ$ to the bending radius rotates such that ϕ decreases as θ increases, causing the shear crevasse to become a transverse crevasse, where $\theta = 90^\circ - 2\phi$. Simple shear in bending parallel flow is analogous to the shear between pages of a book when the book is bent. Axes x, y move with the flowband. Axes θ, r are fixed.

when axes x, y correspond to cylindrical coordinates θ, r :

$$\dot{\epsilon}_{xx} = \dot{\epsilon}_{\theta\theta} = \frac{1}{r} \left(\frac{\partial u}{\partial \theta} + v \right) \simeq \frac{\partial u}{\partial x} = \frac{u'' - u'}{x'' - x'}, \tag{29a}$$

$$\dot{\epsilon}_{yy} = \dot{\epsilon}_{rr} = \frac{\partial v}{\partial r} = \frac{1}{2} \left(\frac{u'' + u'}{x'' - x'} \right) \ln \frac{y''}{y'}, \tag{29b}$$

$$\begin{aligned} \dot{\epsilon}_{xy} = \dot{\epsilon}_{\theta r} &= \frac{1}{2} \left(\frac{\partial u}{\partial r} - \frac{u}{r} + \frac{1}{r} \frac{\partial v}{\partial \theta} \right) \simeq \frac{1}{2} \left(\frac{\partial u}{\partial y} - \frac{u}{r} \right) = \frac{1}{2} \left(-\dot{\theta} - \frac{u}{r} \right) \simeq \\ &\simeq -\frac{1}{2} \left\{ \frac{1}{2} \left(\frac{u'' + u'}{x'' - x'} \right) \theta + \frac{1}{2} \left(\frac{u'' + u'}{r} \right) \right\}. \end{aligned} \tag{29c}$$

Equations (27) and (29) can be combined to give an expression relating strain ϵ_{yy} to $u, \omega,$ and θ .

$$\epsilon_{yy} = \ln \frac{y''}{y'} = 2 \left(\frac{u'' - u'}{u'' + u'} \right) - \frac{\theta}{\tan 2\phi}. \tag{30}$$

If no creep thinning occurs, $\dot{\epsilon}_{zz} = 0$ and bending converging flow is plane strain. By volume

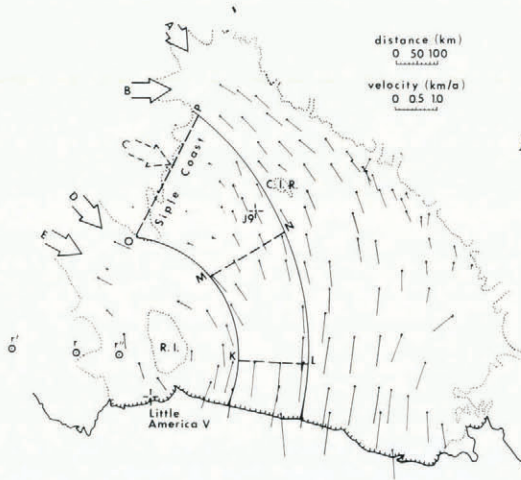


Fig. 7. Bending converging flow on the Ross Ice Shelf. The flow-band from the Siple Coast has a centerline radius r , outer radius r' , and inner radius r'' which do not coincide because flow converges. Bending flow causes velocities along a given radial transect, such as KL, MN, or OP, to be relatively constant. Velocities that increase along a radial transect are localized near grounding lines and form crevasses at 90° to those in Figure 6, as is seen in Figure 2–4 for bending converging flow around Minna Bluff. Flow in Figure 7 differs from flow in Figure 6 in that convergence causes ice to thicken and accelerate, according to Equation (30). Ice velocities are from Bentley and Jezek (1981).

conservation, $\dot{\epsilon}_{xx} = -\dot{\epsilon}_{yy}$ and:

$$\tan 2\phi = \frac{2\dot{\epsilon}_{xy}}{\dot{\epsilon}_{xx} - \dot{\epsilon}_{yy}} = -\frac{\dot{\epsilon}_{xy}}{\dot{\epsilon}_{yy}} = -\frac{\theta}{2 \ln (y''/y')} \tag{31}$$

Combining Equations (30) and (31), no creep thinning gives:

$$\epsilon_{yy} = \ln \frac{y''}{y'} = -\left(\frac{\theta}{2 \tan 2\phi}\right) = -2\left(\frac{u'' - u'}{u'' + u'}\right) \tag{32}$$

Figure 7 shows bending converging flow on the Ross Ice Shelf related to Equation (30). Figure 8 plots ϕ versus θ for various y''/y' ratios in Equation (32).

Table I lists the principal strain-rates obtained from Equations (21), (25), and (30) for the special cases of straight parallel flow ($\dot{\epsilon}_2 = 0$), radially diverging flow ($\dot{\epsilon}_1 = \dot{\epsilon}_2$), simple shear flow ($\dot{\epsilon}_1 = -\dot{\epsilon}_2$), bending diverging flow ($\dot{\epsilon}_3 < 0$), and bending converging flow ($\dot{\epsilon}_3 > 0$). Surface and basal crevasses tend to open along directions perpendicular to principal tensile strain-rates. The orientation of crevasses changes along curving flowlines of the ice shelf, where axis x follows flowlines.

FRACTURE ALONGSIDE ICE STREAMS

When ice streams merge with ice shelves, fracture by shear rupture may occur alongside the floating tongue of an ice stream if it is moving at a surge velocity. Ice streams have a rather rectangular cross-section (Robin and others, 1970). If the thickness h_1 of an ice stream changes an amount Δh_1 in horizontal distance Δx along the ice stream, where $h_1 \gg \Delta h_1$, then the downstream hydrostatic force F_H in an ice stream of width w is

$$F_H = \rho_1 g w h_1 \Delta h_1 \tag{33}$$

provided that the surface slope greatly exceeds the bed slope. This hydrostatic force is resisted by an up-stream shear force F_S given by

$$F_S \approx \tau_0 w \Delta x + 2\tau_s \bar{h}_1 \Delta x \tag{34}$$

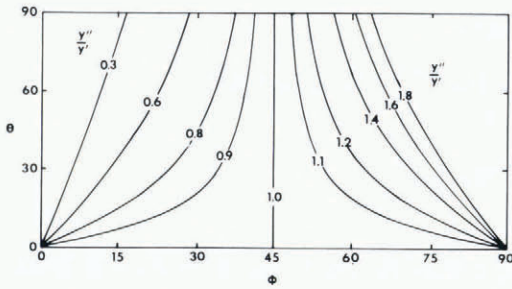


Fig. 8. The effect of longitudinal convergence and divergence on bending flow in an ice shelf with no creep thickening. Crevasses initially open at angles $\phi = 45^\circ$ to the bending radius for all bending angles θ when convergence and divergence are absent, and the subsequent rotation of these crevasses is shown in Figure 6. Converging and diverging flow require that, initially, $\phi < 45^\circ$ and $\phi > 45^\circ$. The value of ϕ is determined by the change in flowband width from y' to y'' as flow bends through angle θ . Equation (32) is plotted for ratios y''/y' from 0.3 to 1.8, where 1.0 is bending parallel flow.

where τ_0 is the basal shear stress, τ_s is the side shear stress, and the ice stream has constant width w and average height $\bar{h}_1 = h_1 + \frac{1}{2}\Delta h_1$. Balancing up-stream forces against down-stream forces and solving for Δh_1 gives

$$\Delta h_1 \simeq \left[\frac{\tau_0 w + 2\tau_s h_1}{P_0 w - \tau_s \Delta x} \right] \Delta x \tag{35}$$

where $P_0 = \rho_1 g h_1$ is the basal hydrostatic pressure. In ice streams, $w \gg h$, τ_0 decreases steadily from a maximum at the head to zero at the flotation/grounding line, and τ_s is relatively constant along its sides. The deviator longitudinal stress gradient $\partial \sigma'_{xx} / \partial x$ is important within 3 km of the grounding line (Sanderson, 1979), so Δx should exceed this distance. Equation (35) simplifies to give the basal shear stress for flow converging at the head of an ice stream, where $\tau_s \rightarrow 0$:

$$\tau_0 \simeq P_0 \Delta h_1 / \Delta x = \rho_1 g h_1 \Delta h_1 / \Delta x, \tag{36}$$

and the lateral shear stress alongside the floating tongue of an ice stream imbedded in an ice shelf, where $\tau_0 = 0$:

$$\tau_s \simeq \frac{1}{2} P_0 (w/h_1) \Delta h_1 / \Delta x = \frac{1}{2} \rho_1 g w \Delta h_1 / \Delta x. \tag{37}$$

Sanderson (1979) has analyzed thickness gradients $\Delta h_1 / \Delta x$ in floating ice.

TABLE I. PRINCIPAL STRAIN-RATES FOR SELECTED ICE-SHELF FLOW CONDITIONS

Principal strain-rates ($n=3$):*	$\dot{\epsilon}_1 / S^{1/n}$	$\dot{\epsilon}_2 / S^{1/n}$	$\dot{\epsilon}_3 / S^{1/n}$
Straight parallel flow ($R=0$):†	$\frac{1}{64}$	0	$-\frac{1}{64}$
Radially diverging flow ($R=+1$):‡	$\frac{1}{72}$	$\frac{1}{72}$	$-\frac{1}{36}$
Pure shear flow ($R=-1$):	$\frac{1}{8}$	$-\frac{1}{8}$	0
Bending diverging flow ($R=-\frac{1}{2}$):	$\frac{4}{81}$	$-\frac{2}{81}$	$-\frac{2}{81}$
Bending diverging flow ($R=+\frac{1}{2}$):	$\frac{7}{500}$	$\frac{7}{1000}$	$-\frac{21}{1000}$
Bending converging flow ($R=-\frac{1}{2}$):‡	$\frac{7}{4}$	$-\frac{21}{8}$	$\frac{7}{8}$

* From Equation (25): $S = \frac{\rho_1 g h_1}{2A} \left(1 - \frac{\rho_1}{\rho_w} \right)$.

† Weertman (1957).

‡ Indeterminate for $R \leq -2$ because $\dot{\epsilon}_1 \rightarrow \infty$ for $R = -2$ and the sign of $\dot{\epsilon}_1$ is positive for even R and negative for odd R when $R < -2$.

The effective stress for an ice stream is

$$\begin{aligned} \tau &= \left[\frac{1}{2} (\sigma'_{xx}{}^2 + \sigma'_{yy}{}^2 + \sigma'_{zz}{}^2 + 2\sigma'_{xy}{}^2 + 2\sigma'_{yz}{}^2 + 2\sigma'_{zx}{}^2) \right]^{1/2} \\ &= \left\{ \frac{1}{2} [\sigma'_{xx}{}^2 + (\dot{\epsilon}_{yy}/\dot{\epsilon}_{xx})^2 \sigma'_{xx}{}^2 + ((-\dot{\epsilon}_{xx} - \dot{\epsilon}_{yy})/\dot{\epsilon}_{xx})^2 \sigma'_{xx}{}^2 + 2(\dot{\epsilon}_{xy}/\dot{\epsilon}_{xx})^2 \sigma'_{xx}{}^2 + \right. \\ &\quad \left. + 2(\dot{\epsilon}_{yz}/\dot{\epsilon}_{xx})^2 \sigma'_{xx}{}^2 + 2(\dot{\epsilon}_{zx}/\dot{\epsilon}_{xx})^2 \sigma'_{xx}{}^2] \right\}^{1/2} \\ &= (1 + R_{yy} + R_{yy}^2 + R_{xy}^2 + R_{yz}^2 + R_{zx}^2)^{1/2} \sigma'_{xx} \\ &\approx (1 + R_{yy} + R_{yy}^2 + R_{xy}^2)^{1/2} \sigma'_{xx} \end{aligned} \quad (38)$$

where $R_{yy} = (\dot{\epsilon}_{yy}/\dot{\epsilon}_{xx})$, $R_{xy} = (\dot{\epsilon}_{xy}/\dot{\epsilon}_{xx})$, $R_{yz} = (\dot{\epsilon}_{yz}/\dot{\epsilon}_{xx})$, $R_{zx} = (\dot{\epsilon}_{zx}/\dot{\epsilon}_{xx})$, and $R_{yz} \approx R_{zx} \approx 0$. From Equation (14):

$$\begin{aligned} \dot{\epsilon}_{xy} &= (\tau^{n-1}/A^n) \sigma'_{xy} \\ &= [(1 + R_{yy} + R_{yy}^2 + R_{xy}^2)^{1/2} (\sigma'_{xy}/R_{xy})]^{n-1} (\sigma'_{xy}/A^n) \\ &= R'' (\sigma'_{xy}/A)^n \end{aligned} \quad (39)$$

where R_{yy} expresses divergence of the floating ice tongue and

$$R'' = [(1 + R_{yy} + R_{yy}^2 + R_{xy}^2)/R_{xy}^2]^{(n-1)/2} \quad (40)$$

The floating tongue of an ice stream imbedded in an ice shelf should have a broad central width w_c where longitudinal strains are important and narrow side widths w_s where simple shear strains dominate. The ice hardness coefficients in these regions are A_c and A_s , respectively, where $A_s \ll A_c$ due to thermal and strain softening in the lateral shear zones. Taking the x -axis along the center-line of the ice stream, u_c as ice velocity at the center-line, u_s as maximum ice velocity in the lateral shear zones, and a linear variation of σ'_{xy} with y so that $\sigma'_{xy} = (2y/w_c)\tau_s$, the variation of longitudinal velocity u_x with y across w_c when $y \leq w_c/2$ is

$$\begin{aligned} u_c - u_x &= \int 2\dot{\epsilon}_{xy} dy = \int_0^y 2R''(\tau_s/A_c)^n (2y/w_c)^n dy \\ &= [2R''(2\tau_s/w_c A_c)^n / (n+1)] y^{n+1}. \end{aligned} \quad (41)$$

Since $u_x = u_s$ at $y = w_c/2$,

$$u_c - u_s = R'' w_c (\tau_s/A_c)^n / (n+1). \quad (42)$$

Subtracting Equation (41) from Equation (42) for $y \leq w_c/2$ gives

$$u_x - u_s = [u_c - u_s][1 - (2y/w_c)^{n+1}]. \quad (43)$$

A simple expression for u_s is obtained if a constant yield stress $\sigma'_{xy} = \tau_s$ exists in lateral shear bands. Simple shear requires that $\dot{\epsilon}_{yy} = 0$ for constant w_s and $\dot{\epsilon}_{xy} \gg \dot{\epsilon}_{xx}$ across w_s , so that $R_{yy} = 0$ and $R_{xy} \gg 1$ gives $R'' \approx 1$ in Equation (40). With constant shear stress, the variation of u_x across w_s when $y \geq w_c/2$ is

$$\begin{aligned} u_s - u_x &= \int 2\dot{\epsilon}_{xy} dy = \int_{w_c/2}^y 2(\tau_s/A_s)^n dy \\ &= (\tau_s/A_s)^n (2y - w_c). \end{aligned} \quad (44)$$

If the lateral shear zones are not rifted, $u_x \rightarrow 0$ at $y = \frac{1}{2}w_c + w_s$ and

$$u_s = 2w_s(\tau_s/A_s)^n. \quad (45)$$

If rifting occurs, $w_s = \tau_s = 0$ and u_s is a lateral sliding velocity equal to the ice-stream velocity.

Rifting occurs when the maximum shear stress τ_m reaches the viscoplastic yield stress σ_v . For simple shear alongside the floating tongue of an ice stream, lateral rifts open when, from the Mohr circle,

$$\sigma_v = \frac{1}{2}(\sigma_1 - \sigma_2) = [\frac{1}{4}(\sigma_{xx} - \sigma_{yy})^2 + \sigma_{xy}^2]^{1/2} \approx \sigma_{xy} = \tau_s. \quad (46)$$

An ice stream punching into an ice shelf experiences compressive flow until it can punch through the ice shelf. Compressive flow causes the floating ice tongue to diverge laterally, so that R_{yy} is negative in Equation (40) and u_s decreases in Equation (45). The lateral rifts remain open until u_s decreases enough so that $\tau_s < \sigma_v$, where τ_s is given by Equation (37) and σ_v is given by either Equation (8) or Equation (10). In Antarctica, an estimate of σ_v can be made at the down-stream end of the lateral rifts created where Byrd Glacier punches into the Ross Ice Shelf. Lateral divergence of the floating ice tongue of amount $R_{yy} \approx -2.2$ allows ice thinning of $\Delta h_1 \approx 200$ m over rifted length $\Delta x \approx 40$ km and average width $w \approx 35$ km (Hughes, 1977). Entering these values into Equation (37) gives $\sigma_v \approx 8$ bars for strain-softened fracture at the ends of rifts. As shown in Figure 9, these rifts can allow ice streams to punch through their confining ice shelf.

FRACTURE ALONG GROUNDING LINES

An ice shelf cannot effectively resist the punch of a surging ice stream unless the ice shelf occupies a confined embayment and is pinned to bedrock at ice rises in the embayment. However, the links between the ice shelf and the ice rises are weak, as is the link to bedrock along grounding lines of the embayment. These links are weakened primarily by repeated tidal flexure (Swithinbank, 1955; Robin, 1958), but also by shear rupture where the ice shelf moves parallel to grounding lines in the embayment and alongside ice rises (Thiel and Ostenso, 1961; Barrett, 1975). Shear rupture alongside these grounding lines can be analyzed in much the same way as shear rupture alongside the floating tongues of ice streams imbedded in the ice shelf. Our analysis of fracture along grounding lines, therefore, will focus on fatigue rupture caused by cyclic tidal flexure.

Crevasse open normal to the largest tensile principal stress, and a depression along ice shelf grounding lines (Swithinbank, 1955) suggests necking associated with the maximum tensile stress caused by tidal bending. In a tensile test, the applied force F does not change at the upper yield stress σ_v when the strain of viscoplastic instability ϵ_v is inhomogeneous. This causes localized recrystallization and necking, which terminates in a cup-and-cone fracture for a circular cross-section. An ice shelf has a rectangular cross-section. Let x be the horizontal distance normal to its grounding line, y be the horizontal distance along its grounding line, and z be the vertical distance upward, with the origin of coordinates x, y, z at the neutral axis, taken as midway through the ice shelf. Actually, the vertical density gradient in ice shelves displaces the neutral axis toward the base (Gow, 1963). Necking along the grounding line is caused by the maximum surface and basal tensile stresses σ_m during tidal bending. If tidal bending force F_x stretches length L_x and reduces cross-sectional area A_x normal to x , where volume $L_x A_x$ is

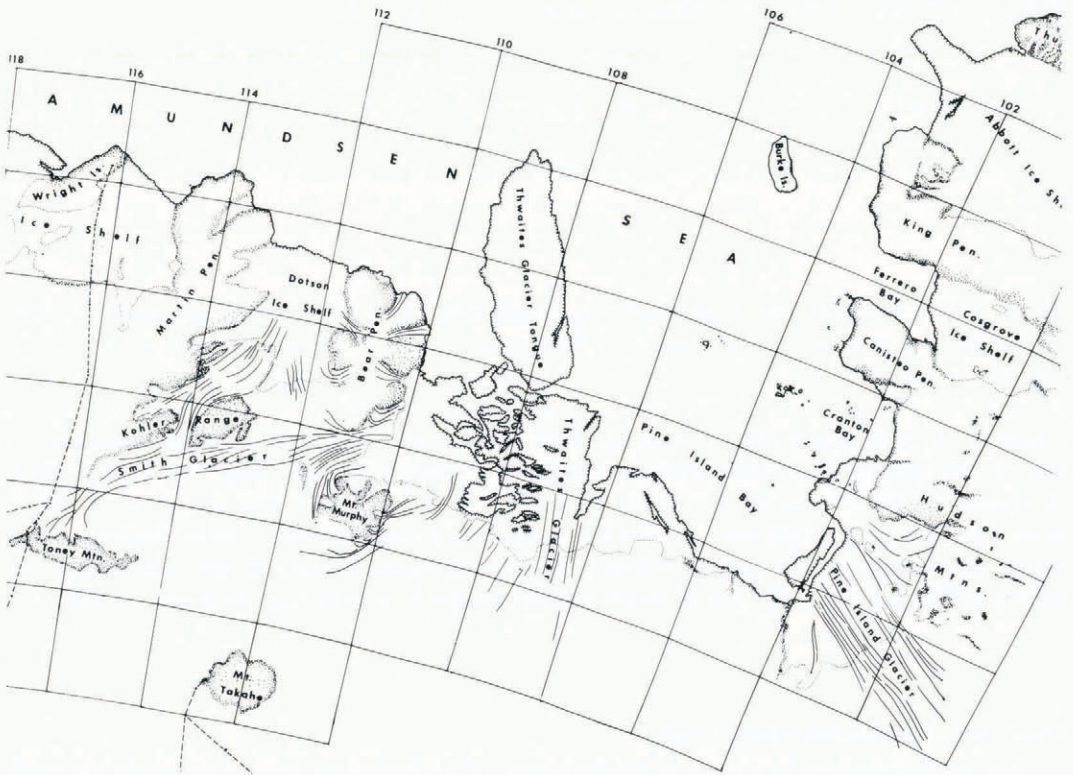


Fig. 9. Ice streams and ice shelves on the Amundsen Sea flank of the West Antarctic ice sheet. Thwaites Glacier and Pine Island Glacier have punched through an ice shelf in Pine Island Bay, presumably because the length of their lateral rifts is comparable to the distance from the calving front (hatched lines) to the grounding line (dotted lines) of the ice shelf. A comparison of 1947 trimetrogon photography with 1972 Landsat imagery shows that Thwaites Glacier tongue has buckled laterally in mode $N=1$, and is now rotating about a probable pinning point about 200 km from its grounding line. This rotation was first noted by Robert J. Allen (personal communication, May 1978).

conserved, the necking condition for viscoplastic yielding requires that

$$dF_x = d(A_x \sigma_v) = A_x d\sigma_v + \sigma_v dA_x = 0. \quad (47)$$

Separate expressions for the change in strain at the viscoplastic yield stress σ_v are obtained from Equations (1) and (47), putting $\sigma = \sigma_v$ and $\varepsilon = \varepsilon_v$ in Equation (1),

$$d\varepsilon_v = d(\sigma_v/\sigma_s)^s = s\sigma_v^{s-1} d\sigma_v/\sigma_s^s = dL_x/L_x = -dA_x/A_x = d\sigma_v/\sigma_v. \quad (48)$$

Equation (48) reduces to the following relationship between σ_s and σ_v :

$$\sigma_s^s = s\sigma_v^s. \quad (49)$$

By comparing Equations (1) and (49) it is clear that $\varepsilon_v = 1/s$. As seen in Figure 3, however, $s \rightarrow 0$ at $\varepsilon = \varepsilon_v$ and this requires that $\sigma_s \rightarrow 0$ in Equation (49). Consequently, a fracture analysis for tidal flexure must consider conditions of homogeneous strain that exist just prior to necking. These would be conditions of parabolic strain-hardening for which $s=2$ is observed.

Bending stress σ_{xx} caused by tidal flexure varies linearly with distance h_0 from the neutral axis of the ice shelf, which is taken at the mid-point of an ice shelf having thickness h_1 . The bending strain ϵ_{xx} at distance h_0 from the neutral axis is, for elastic bending:

$$\epsilon_{xx} = \sigma_{xx}/\sigma_e = h_0/R_e \tag{50}$$

where σ_e is the elastic modulus and R_e is the radius of strain curvature for elastic bending given by

$$\frac{1}{R_e} = \frac{d^2z/dx^2}{[1 + (dz/dx)^2]^{3/2}} \simeq \frac{d^2z}{dx^2} \tag{51}$$

Pinned boundary conditions along the grounding line require that $z = dz/dx = 0$ at $x = 0$, and $z = z_m$ as $x \rightarrow \infty$ is the maximum vertical tidal displacement of the ice shelf. These boundary conditions require that the ice shelf is not in hydrostatic equilibrium except at mean tide. With departures from mean tide, a vertical shear stress σ_{zx} is induced by shearing force F_z , where:

$$\sigma_{zx} = dF_z/dx = d^2M/dx^2 = \rho_w g(z_m - z) \tag{52}$$

By definition, $F_z = dM/dx$ where M is the bending moment.

During tidal flexure resulting in elastic strain and strain-hardening, the longitudinal bending strain ϵ_{xx} is related to the longitudinal bending stress σ_{xx} by writing Equation (1) for the tidal flexure application in the form

$$\epsilon_{xx} = (\sigma_{xx}/\sigma_s)^s \tag{53}$$

where $\sigma_s = \sigma_e$ and $s = 1$ for elastic bending, and $\sigma_e > \sigma_s > \sigma_v$ and $s = 2$ for parabolic strain-hardening (Hughes, 1977). Using Equations (43) and (51), the bending moment is:

$$\begin{aligned} M &= \int_{-h_1/2}^{+h_1/2} \sigma_{xx} h_0 \, dh_0 = \int_{-h_1/2}^{+h_1/2} \sigma_s (\epsilon_{xx})^{1/s} h_0 \, dh_0 \\ &= \int_0^{h_1} \sigma_s (h_0/R_e)^{1/s} h_0 \, dh_0 = \frac{\sigma_s h_1^{2+1/s}}{(2+1/s)R_e^{1/s}} \end{aligned} \tag{54}$$

Combining Equations (44) and (52) to get the bending curvature

$$\frac{d^2z}{dx^2} = \left[\frac{(2+1/s)M}{\sigma_s h_1^{2+1/s}} \right]^s \tag{55}$$

Differentiating twice more

$$\frac{d^4z}{dx^4} = \left[\frac{2+1/s}{\sigma_s h_1^{2+1/s}} \right] \left[(s-1)sM^{s-2} \left(\frac{dM}{dx} \right)^2 + sM^{s-1} \left(\frac{d^2M}{dx^2} \right) \right] \tag{56}$$

The general solution for elastic strain is obtained by setting $s = 1$ and integrating. The elastic displacement, first solved by Robin (1958), is

$$z_e = z_m - (C_1 \cos \lambda_e x + C_2 \sin \lambda_e x) \exp(\lambda_e x) + (C_3 \cos \lambda_e x + C_4 \sin \lambda_e x) \exp(-\lambda_e x) \tag{57}$$

where

$$\lambda_e = (3\rho_w g/\sigma_e h_1^3)^{1/4} \tag{58}$$

is the elastic damping factor. The general solution for parabolic strain-hardening is obtained by setting $s = 2$ and integrating. The viscoplastic displacement is

$$z_v = (K/8\lambda_v^2)(2 - \cos 2\lambda_v x) \exp(-2\lambda_v x) + C_5 x + C_6 \quad (59)$$

where λ_v is the viscoplastic damping factor and

$$K = (6\rho_w g z_m^2 \sigma_e / h_1^2 \sigma_v). \quad (60)$$

Since elastic and viscoplastic strains are additive, the total bending displacement is the sum of Equations (57) and (59):

$$z = z_e + z_v \approx z_m - [(z_m + K/8\lambda_v^2) \cos \lambda_e x] \exp(-\lambda_e x) - [(z_m - K/8\lambda_v^2) \sin \lambda_e x] \exp(-\lambda_e x) + (K/8\lambda_v^2)(2 - \cos 2\lambda_v x) \exp(-2\lambda_v x) \quad (61)$$

where $C_1 = C_2 = C_5 = 0$ since z is finite, $C_6 = 0$ since $z = z_m$ as $x \rightarrow \infty$, $C_3 = z_m + K/8\lambda_v^2$ since $z = 0$ at $x = 0$, and $C_4 = z_m - K/8\lambda_v^2$ since $dz/dx = 0$ at $x = 0$. Equation (59) results from an attempt to involve strain-hardening in tidal flexure (Hughes, 1977; Lingle, unpublished; Lingle and others, 1981).

Lingle and others (1981) studied the tidal flexure of Jacobshavn Isbrae in Greenland. By setting $\lambda_v = \lambda_e$ and $z_m = K/8\lambda_v^2$ in Equation (61), a good fit to flexure data was obtained. Equation (61) then reduces to:

$$z = z_m [1 - 2 \cos \lambda_e x \exp(-\lambda_e x) + (2 - \cos 2\lambda_e x) \exp(-2\lambda_e x)]. \quad (62)$$

Lingle and others (1981) computed $\sigma_m \approx 5$ bars at the side grounding line and $\sigma_m \approx 1$ bar at the second stress maximum for ice in which fatigue fracture has given an uncrevassed ice thickness of 160 ± 48 m in floating ice 750 m thick, where $\sigma_e/\sigma_s = 247 \pm 37$ for strain-hardened fracture.

BUCKLING UP-STREAM FROM ICE RISES

An ice rise most effectively pins an ice shelf by resisting up-stream flow, rather than lateral or down-stream flow. Since an ice shelf is thin compared to its width and length, pushing against an ice rise may cause the ice shelf to buckle instead of thickening uniformly. If so, the compressive force should be analyzed in terms of buckling in a thin sheet. Consider an ice rise having radius r and resisting an up-stream longitudinal force F_x from the ice shelf. Buckling begins with a small vertical displacement z , possibly due to tidal changes. Bending stress σ_{xx} varies linearly with distance h_0 . The bending moment M , where $\sigma_{xx} = \sigma_m$ at the surface and the base, is

$$M = F_x z = \int_0^{h/2} [(2h_0/h_I)\sigma_m][2r dh_0] h_0 = \frac{1}{6} r h_1^2 \sigma_m. \quad (63)$$

From Equations (50) and (51) the maximum bending strain is

$$\epsilon_m = \sigma_m/\sigma_e = h_1/2R_e = \frac{1}{2} h_1 (d^2 z/dx^2). \quad (64)$$

Substituting for σ_m from Equation (63),

$$d^2 z/dx^2 = K^2 z \quad (65)$$

where the compressive stress is $\sigma_c = F_x/2rh_1$ and

$$K^2 = 12F_x/rh_1^3\sigma_e = 24\sigma_c/\sigma_e h_1^2. \quad (66)$$

The solution of Equation (65) is

$$z = C_1 \sin(Kx) + C_2 \cos(Kx) = C_1 \sin(N\pi x/L) \quad (67)$$

where L is the length of the ice shelf which buckles, N is the number of bends that occur in that length, $K = N\pi/L$ from the boundary condition that $z = 0$ at $x = L$ and $C_2 = 0$ from the boundary condition that $z = 0$ at $x = 0$. The compressive stress needed to cause buckling is

$$\sigma_c = K^2 h_1^2 \sigma_e / 24 = (N\pi h_1 / L)^2 \sigma_e / 24. \quad (68)$$

Vertical buckling must overcome a body force due to gravity, and vertical displacement z is reduced if N is large. However, increasing N increases σ_c . Lateral buckling is not retarded by the body force, so it occurs for $N = 1$ and σ_c is minimized. However, lateral buckling is possible only if the ice rise pins the floating tongue of an ice stream that is not imbedded in a confined ice shelf. In Antarctica, the floating tongue of Thwaites Glacier seems to have punched through an ice shelf and it has buckled laterally in the mode $N = 1$, seen in Figure 9, and the Brunt Ice Shelf has buckled vertically in the mode $N \approx 10$ up-stream from an ice rise (Thomas, 1973, plate IIIa). Taking $\sigma_e \approx 9.7 \times 10^4$ bars in Equation (68), $L \approx 200$ km and $h_1 \approx 500$ m gives $\sigma_c \approx 0.23$ bar for Thwaites Glacier, and $L \approx 70$ km and $h_1 \approx 170$ m gives $\sigma_c \approx 23.5$ bars for the Brunt Ice Shelf. Converging flow in an ice shelf confined in an embayment may also cause transverse buckling that would create longitudinal undulations (Hughes, 1972, p. 53–55).

DISCUSSION

The reason for studying the role of fracture in ice-shelf dynamics is better to understand the stability of Antarctic ice shelves, particularly those that buttress the marine West Antarctic ice sheet, which is believed to be inherently unstable (Hughes, 1972; Weertman, 1974). An ice shelf is probably metastable; it can survive small temporary perturbations but not large prolonged ones. For a given surface and basal mass balance, it exists so long as the supply of ice crossing its grounding lines is able to replace ice lost along its calving front.

Ice rises and islands typically pin an ice shelf along its calving front, and actually determine the position of the calving front along a line across which the ice discharge velocity matches the iceberg calving rate (Swithinbank, 1955). Any process, such as rising sea-level or surface and basal melting, that floats the ice shelf free from its pinning points reduces the ice discharge velocity by increasing the calving perimeter. A calving bay will then carve away the ice shelf until other ice rises establish a new calving front where ice discharge again matches iceberg calving.

If the new calving front is too close to the grounding line of the ice shelf, ice streams can punch through the ice shelf and surge (see Figures 2–6 and 9). This has two consequences. First, deprived of ice input from these surging ice streams, the mass balance of the ice shelf will turn strongly negative so that the discharge velocity at the calving front falls behind the iceberg calving rate. This allows the calving bay to migrate past the array of ice rises and continue to carve away the ice shelf. Second, being no longer buttressed by the ice shelf, the ice streams will not only be able to surge, the surges can be more vigorous and prolonged so that more interior ice will be drawn down into the ice streams. This compels the grounding line to retreat into the

ice sheet at the same time that the calving bay is advancing into the ice shelf. Survival of the ice shelf depends upon which retreat rate is greatest.

The consequences of fracture on the stability of an ice shelf, and ultimately on the stability of the West Antarctic ice sheet, may even now be unfolding. Most of the ice draining from the northern flank of the West Antarctic ice sheet is drawn down into Pine Island Bay through Thwaites and Pine Island Glaciers, two huge ice streams that have apparently punched through a confined and pinned ice shelf and are now surging. The disintegration scenario outlined here for ice shelves may have already been played out in Pine Island Bay (Stuiver and others, 1981; Hughes, 1981).

MS. received 6 May 1981 and in revised form 15 April 1982

REFERENCES

- American Geographical Society. 1970. Antarctica. *World 1:5,000,000*. Sheet 13. New York, American Geographical Society.
- Baker, R. W. 1981. Textural and crystal-fabric anisotropies and the flow of ice masses. *Science*, Vol. 211, No. 4486, p. 1043–44.
- Barrett, P. J. 1975. Seawater near the head of the Ross Ice Shelf. *Nature*, Vol. 256, No. 5516, p. 390–92.
- Bentley, C. R., and Jezek, K. C. 1981. RISS, RISP, and RIGGS: post-IGY glaciological investigations of the Ross Ice Shelf in the U.S. programme. *Journal of the Royal Society of New Zealand*, Vol. 11, No. 4, p. 355–72.
- Clough, J. W. 1974. RISP radio-echo sounding. *Antarctic Journal of the United States*, Vol. 9, No. 4, p. 159.
- Dieter, G. E. 1961. *Mechanical metallurgy*. New York, McGraw-Hill Book Co., Inc.
- Fastook, J. L., and Schmidt, W. F. 1982. Finite element analysis of calving from ice fronts. *Annals of Glaciology*, Vol. 3, p. 103–06.
- Glen, J. W. 1958. The flow law of ice: a discussion of the assumptions made in glacier theory, their experimental foundations and consequences. *Union Géodésique et Géophysique Internationale. Association Internationale d'Hydrologie Scientifique. Symposium de Chamonix, 16–24 sept. 1958*, p. 171–83. (Publication No. 47 de l'Association Internationale d'Hydrologie Scientifique.)
- Gow, A. J. 1963. The inner structure of the Ross Ice Shelf at Little America V, Antarctica, as revealed by deep core drilling. *Union Géodésique et Géophysique Internationale. Association Internationale d'Hydrologie Scientifique. Assemblée générale de Berkeley, 19–8–31–8 1963. Commission des Neiges et des Glaces*. p. 272–84. (Publication No. 61 de l'Association Internationale d'Hydrologie Scientifique.)
- Hughes, T. J. 1972. Is the West Antarctic ice sheet disintegrating? *ISCAP Bulletin* (Ohio State University), No. 1.
- Hughes, T. J. 1977. West Antarctic ice streams. *Reviews of Geophysics and Space Physics*, Vol. 15, No. 1, p. 1–46.
- Hughes, T. J. 1979. Byrd Glacier. *Antarctic Journal of the United States*, Vol. 14, No. 5, p. 88–91.
- Hughes, T. J. 1981. The weak underbelly of the West Antarctic ice sheet. *Journal of Glaciology*, Vol. 27, No. 97, p. 518–25. [Letter.]
- Lingle, C. S. Unpublished. Tidal flexure of Jakobshavns Glacier, west Greenland. [M.S. thesis, University of Maine, 1978.]
- Lingle, C. S., and others. 1981. Tidal flexure of Jakobshavns Glacier, west Greenland, by C. S. Lingle, T. [J.] Hughes, and R. C. Kollmeyer. *Journal of Geophysical Research*, Vol. 86, No. B5, p. 3960–68.
- Nye, J. F. 1960. *Physical properties of crystals: their representation by tensors and matrices*. London, Oxford University Press.
- Pfeffer, W. T. 1982. The effect of crevassing on the radiative absorptance of a glacier surface. *Annals of Glaciology*, Vol. 3, p. 353. [Abstract.]
- Robin, G. de Q. 1958. Glaciology. III. Seismic shooting and related investigations. *Norwegian–British–Swedish Antarctic Expedition, 1949–52. Scientific Results*, Vol. 5.
- Robin, G. de Q., and others. 1970. Radio-echo sounding of the Antarctic ice sheet, by G. de Q. Robin, S. Evans, D. J. Drewry, C. H. Harrison, and D. L. Petrie. *Antarctic Journal of the United States*, Vol. 5, No. 6, p. 229–32.
- Sanderson, T. J. O. 1979. Equilibrium profile of ice shelves. *Journal of Glaciology*, Vol. 22, No. 88, p. 435–60.

- Stuiver, M., *and others*. 1981. History of the marine ice sheet in West Antarctica during the last glaciation: a working hypothesis, by M. Stuiver, G. H. Denton, T. [J.] Hughes, and J. L. Fastook. (In Denton, G. H., *and* Hughes, T. J., ed. *The last great ice sheets*. New York, Wiley-Interscience, p. 319–436.)
- Swithinkbank, C. W. M. 1955. Ice shelves. *Geographical Journal*, Vol. 121, Pt. 1, p. 64–76.
- Thiel, E., *and* Ostenso, N. A. 1961. The contact of the Ross Ice Shelf with the continental ice sheet. Antarctica. *Journal of Glaciology*, Vol. 3, No. 29, p. 823–32.
- Thomas, R. H. 1973. The dynamics of the Brunt Ice Shelf, Coats Land, Antarctica. *British Antarctic Survey. Scientific Reports*, No. 79.
- Weertman, J. 1957. Deformation of floating ice shelves. *Journal of Glaciology*, Vol. 3, No. 21, p. 38–42.
- Weertman, J. 1973. Can a water-filled crevasse reach the bottom surface of a glacier? *Union Géodésique et Géophysique Internationale. Association Internationale d'Hydrologie Scientifique. Commission de Neiges et Glaces. Symposium on the Hydrology of Glaciers, Cambridge, 7–13 September 1969*, p. 139–45. (Publication No. 95 de l'Association Internationale d'Hydrologie Scientifique.)
- Weertman, J. 1974. Stability of the junction of an ice sheet and an ice shelf. *Journal of Glaciology*, Vol. 13, No. 67, p. 3–11.
- Weertman, J. 1980. Bottom crevasses. *Journal of Glaciology*, Vol. 25, No. 91, p. 185–88.